

Numerical investigation of frequency spectrum in the Hasegawa-Wakatani model

Juhyung Kim and P. W. Terry

Citation: *Phys. Plasmas* **20**, 102303 (2013); doi: 10.1063/1.4822335

View online: <http://dx.doi.org/10.1063/1.4822335>

View Table of Contents: <http://pop.aip.org/resource/1/PHPAEN/v20/i10>

Published by the AIP Publishing LLC.

Additional information on Phys. Plasmas

Journal Homepage: <http://pop.aip.org/>

Journal Information: http://pop.aip.org/about/about_the_journal

Top downloads: http://pop.aip.org/features/most_downloaded

Information for Authors: <http://pop.aip.org/authors>

ADVERTISEMENT

AIP | Applied Physics Letters

SURFACES AND INTERFACES
Focusing on physical, chemical, biological, structural, optical, magnetic and electrical properties of surfaces and interfaces, and more...

ENERGY CONVERSION AND STORAGE
Focusing on all aspects of static and dynamic energy conversion, energy storage, photovoltaics, solar fuels, batteries, capacitors, thermoelectrics, and more...

EXPLORE WHAT'S NEW IN APL

SUBMIT YOUR PAPER NOW!

Numerical investigation of frequency spectrum in the Hasegawa-Wakatani model

Juhyung Kim^{1,a)} and P. W. Terry²

¹*Department of Physics, Korea Advanced Institute of Science and Technology, Daejeon 305-701, Republic of South Korea*

²*Department of Physics, University of Wisconsin-Madison, Madison, Wisconsin, 53706, USA*

(Received 10 July 2013; accepted 4 September 2013; published online 2 October 2013)

The wavenumber-frequency spectrum of the two-dimensional Hasegawa-Wakatani model is investigated in the hydrodynamic, intermediate, and adiabatic regimes. A nonlinear frequency and a line width related to energy transfer properties provide a measure of the average frequency and spectral broadening, respectively. In the adiabatic regime, narrow spectra, typical of wave turbulence, are observed with a nonlinear frequency shift in the electron drift direction. In the hydrodynamic regime, broad spectra with almost zero nonlinear frequencies are observed. Nonlinear frequency shifts are shown to be related to nonlinear energy transfer by vorticity advection through the high frequency region of the spectrum. In the intermediate regime, the nonlinear frequency shift for density fluctuations is observed to be weaker than that of electrostatic potential fluctuations. The weaker frequency shift of the density fluctuations is due to nonlinear density advection, which favors energy transfer in the low frequency range. Both the nonlinear frequency and the spectral width increase with poloidal wavenumber k_y . In addition, in the adiabatic regime where the nonlinear interactions manifest themselves in the nonlinear frequency shift, the cross-phase between the density and potential fluctuations is observed to match a linear relation, but only if the linear response of the linearly stable eigenmode branch is included. Implications of these numerical observations are discussed. © 2013 AIP Publishing LLC. [<http://dx.doi.org/10.1063/1.4822335>]

I. INTRODUCTION

Wave turbulence is a widely occurring phenomenon in plasma and fluid systems across various intrinsic temporal and spatial scales.^{1,2} Wave (weak) turbulence is typically characterized by a linear auto-correlation time that is shorter than the nonlinear decorrelation time as determined from random fluctuations.³ Strong turbulence⁴ lies in the opposite limit where the decorrelation process is nonlinear.³ Weak and strong turbulence regimes provide a good conceptual basis for understanding turbulent fluctuations in theoretical and experimental setups. Of particular interest is the frequency spectrum, which when subjected to detailed analysis, can provide insights on turbulence beyond those of wavenumber analysis. Such insights can be expected to provide benefits toward eventual control and utilization of plasma turbulence.

The frequency spectra of turbulent fluctuations $P(\omega)$ are straightforward to obtain in fusion experiments because of the ease of producing time series from measurement diagnostics. However, theoretical models are more likely to produce wavenumber spectra $P(\mathbf{k})$ because of unambiguous relationships to spectral energy transfer. Frequency spectra can be produced from numerical solutions, but their interpretation, especially in terms of fluctuation constituents, is not a simple matter. Better understanding of the wavenumber-frequency spectrum $P(\omega, \mathbf{k})$ would be helpful to bridge experiment and theory. The simplest possible mapping between the wavenumber spectrum and the frequency spectrum would be quasilinear, $\omega = \omega_\ell(k)$ where ω_ℓ is a linear

eigenmode frequency for micro-instabilities at energetically dominant wavenumbers. However, the true relationship between wavenumber and frequency can be intractably complicated.^{5,6} Moreover, where multiple instabilities occur over a range of wavenumbers, the frequencies of fluctuations need not bear a simple relationship to the instabilities. [For example, see Fig. 10(B) of Ref. 7. While the trapped-electron mode (TEM) is unstable at the mid-range, the mean frequency is in the ion direction and appears to be extended from the ion-temperature-gradient mode (ITG) at the lower wavenumbers.]

Recent studies of plasma turbulence that account for the spectrum of “damped” modes offer new insight on the mode frequency input to plasma turbulence. These studies have shown that damped modes play a key role in saturated turbulence even at the length scale of instability.^{6,8–11} Damped modes excited by the nonlinearity in large numbers may carry a real frequency (see Fig. 2 of Ref. 11) so that potentially a large number of linear time scales might enter into the frequency spectrum at a fixed wavenumber. In addition to these linear frequencies, there can be nonlinear frequency shifts associated with consistent nonlinear energy transfer among the modes.¹² There have been recent investigations to explore nonlinear effects on the frequency spectrum, such as energy transfer among fluctuations of different frequencies.¹³ While these studies clearly demonstrate a similar energy transfer in the wavenumber and frequency spectrum, for the most part these spectra are specified as either the frequency spectrum $P(\omega, x_0)$ at a fixed spatial location or the wavenumber spectrum $P(\mathbf{k}, t_0)$ at a fixed time, making comparison difficult.

^{a)}Electronic mail: yegakjh@kaist.ac.kr

The frequency spectrum at a large wavenumber $k = |\mathbf{k}|$ is expected to be broad. Fluctuations are highly nonlinear at those wavenumbers and can be typically modeled as a turbulent diffusion. Energy transfer in wavenumber space is strongly nonlinear and balances the total energy injection into the system to achieve a steady state. Kim and Terry¹² have shown that three-wave coupling with complex frequencies (i.e., including linear growth rates) in a generalized one-fluid model can have a finite nonlinear frequency shift relative to linear frequencies. This emerges through nonlinear energy transfer and cannot be explained by turbulent diffusion, i.e., by frequency broadening. Can nonlinear frequencies be identified in more general models, such as fluid models with two or more fields, or gyrokinetic models? Are those frequencies related to nonlinear energy transfer? We investigate the $P(\omega, \mathbf{k})$ spectrum and nonlinear frequencies in the Hasegawa-Wakatani (HW) model as a step toward answering these questions.

The HW model,¹⁴ which describes parallel collisional drift wave turbulence in a minimal and self-consistent way, is well-known to span *weak* ($\tilde{\omega} \gg \Delta\tilde{\omega}$) and *strong* ($\tilde{\omega} \ll \Delta\tilde{\omega}$) turbulence regimes, where $\tilde{\omega}$ and $\Delta\tilde{\omega}$ are the nonlinear frequency and the spectral width. Gang *et al.*¹⁵ constructed the equations for the correlation functions via the eddy-damped quasi normal Markovian (EDQNM) closure¹⁶ and showed that the phase locked cross-correlation between density and potential with $n \sim \phi$ inhibits density advection in the adiabatic regime. In the hydrodynamic regime, the disruption of this strong correlation leads to a coherent structure where the density fluctuation is trapped within vorticity. In their analysis, only the frequency broadening is included, while assuming $\tilde{\omega} \sim \omega_e$. Hu *et al.*¹⁷ describe HW turbulence in an EDQNM closure systemically derived from the Direct Interaction Approximation (DIA)^{18,19} and show the smooth transition from weak to strong turbulence in terms of the adiabaticity parameter. While the DIA closure does not exclude the nonlinear deviation of frequency from the linear frequency, it has never been clearly shown. Futatani *et al.*²⁰ analyze the statistics of vorticity in the intermediate regime focusing on the low-mode-number description of the turbulence. Our focus is the description of the nonlinear frequency $\tilde{\omega}$ and $\Delta\tilde{\omega}$ in the hydrodynamic and adiabatic regimes.

In this paper, the frequency spectrum is investigated numerically. Our findings are that the electrostatic potential and electron density fluctuations can have finite nonlinear frequencies ($\neq \omega_{\text{lin}}$), and the nonlinear frequencies of each field can be distinct in some regimes. The frequency shifts can be related to nonlinear energy transfer; therefore, the nonlinear frequency shift may be included in more refined wave turbulence theory, and as a comparison-measure for model validation using experimental measurements.

The HW model is introduced and linear analysis is presented in Sec. II. A spectrum model from which nonlinear frequencies and spectral widths can be obtained from the frequency spectrum is presented in Sec. III, along with related numerical findings. In Sec. IV, a theoretical framework for interpreting the findings is presented and the implications are discussed. The final conclusion is given in Sec. V.

II. HASEGAWA-WAKATANI MODEL

In a shearless plane slab geometry with a constant magnetic field \mathbf{B} pointing in the z direction, the two-field HW model²¹ for the normalized electrostatic potential $\phi \equiv (L_n/\rho_s)(e\tilde{\phi}/T_e)$ and density $\psi \equiv (L_n/\rho_s)(\tilde{n}/n_0)$ can be written as follows:

$$\begin{aligned} \frac{d}{dt} \nabla_{\perp}^2 \phi &= \alpha(\phi - \psi) + \nu \nabla_{\perp}^2 \nabla_{\perp}^2 \phi, \\ \frac{d}{dt} \psi &= \alpha(\phi - \psi) - \kappa \frac{\partial \phi}{\partial y} + \mu \nabla_{\perp}^2 \psi, \end{aligned} \quad (1)$$

where

$$\frac{d}{dt} = \frac{\partial}{\partial t} + \mathbf{v}_E \cdot \nabla_{\perp} \text{ and}$$

$$\mathbf{v}_E = \hat{\mathbf{z}} \times \nabla_{\perp} \phi,$$

$\alpha \equiv (L_n/\rho_s)k_{\parallel}^2 v_e^2 / (\nu_{ei} \omega_{ci})$, v_e is the electron thermal velocity, ν_{ei} is the electron-ion collision frequency, ω_{ci} is the ion cyclotron frequency, $\rho_s = c_s/\omega_{ci}$ is the ion sound gyroradius, $\omega_{ci} = eB/m_i$ is the ion cyclotron frequency, $L_n = d \log n_e / dr$ is the electron density gradient, and ν and μ are the collisional viscosity and diffusivity, respectively. Time and length are normalized to c_s/L_n and ρ_s , and the normalized density gradient κ controls the drift wave frequency. There are two nonlinear terms, vorticity advection $\mathbf{v}_E \cdot \nabla_{\perp} \nabla_{\perp}^2 \phi$ and density advection $\mathbf{v}_E \cdot \nabla_{\perp} \psi$. The adiabatic parameter α characterizes the degree to which electrons can move rapidly along the magnetic field lines and establish an approximate adiabatic response $\psi \sim \phi$, making the density advection negligible. The HW model exhibits both an adiabatic regime ($\alpha \gg 1$) and a hydrodynamic regime ($\alpha \ll 1$).¹⁵ In the model, the cross-phase between the potential ϕ and the density ψ evolves dynamically and self-consistently, compared to the one-field Terry-Horton²² model with a fixed cross-phase defined by the unstable linear mode. In the strict adiabatic limit where $\alpha \rightarrow \infty$, electron density fluctuations are adiabatic, $\psi \rightarrow \phi$, and the HW model reduces to a Hasegawa-Mima (HM) equation.²³ This purely adiabatic limit does not produce any transport.

In wavenumber space, the set of the equations is written as

$$\begin{aligned} \frac{\partial \phi}{\partial t} &= -\frac{\alpha}{k^2}(\phi - \psi) - \nu k^2 \phi + \frac{1}{2} \frac{\hat{\mathbf{z}} \cdot \mathbf{k}' \times \mathbf{k}'' (k'^2 - k''^2)}{k^2} \phi' \phi''^*, \\ \frac{\partial \psi}{\partial t} &= \alpha(\phi - \psi) - i\omega_* \phi - \mu k^2 \psi + \frac{1}{2} \hat{\mathbf{z}} \cdot \mathbf{k}' \times \mathbf{k}'' (\phi' \psi''^* - \phi''^* \psi'^*), \end{aligned} \quad (2)$$

where ϕ and ψ are the potential and density at wavenumber k , ϕ' and ψ' are at wavenumber k' , and ϕ'' and ψ'' are at wavenumber $k'' = k - k'$. Terms that depend on k' (and k'') have an implicit sum over k' , and $\omega_* = k_y \kappa$. The complex linear eigen-frequencies ω are

$$\begin{aligned} \omega_{1,2} &= -\frac{i}{2} \left[\alpha \left(1 + \frac{1}{k^2} \right) + (\nu + \mu) k^2 \right] \\ &\quad \pm \frac{i}{2} \left\{ \left[\alpha \left(1 - \frac{1}{k^2} \right) - (\nu - \mu) k^2 \right]^2 + \frac{4\alpha}{k^2} (\alpha - i\omega_*) \right\}^{1/2}. \end{aligned} \quad (3)$$

There are two eigenmode branches, an unstable branch of frequency ω_1 and a stable branch of frequency ω_2 . The Fourier modes on the stable branch are always stable, $\text{Im } \omega_{\text{lin},2} < 0$, whereas the modes on the unstable branch are unstable only for a limited wavenumber range corresponding to large scale. Given the linear eigen-frequencies $\omega_{1,2}$, the ratios between two fields, which define the eigenvectors, are

$$\beta_{1,2} = \left(\frac{\psi}{\phi} \right)_{1,2} = \frac{1 - i\omega_*/\alpha}{1 - i\omega_{1,2}/\alpha + \mu k^2/\alpha} = 1 - i\omega_{1,2}k^2/\alpha + \nu k^4/\alpha. \quad (4)$$

In the adiabatic regime where $\alpha \gg \omega_{\text{lin}}, \omega_*, \mu k^2$ and νk^2 , the complex ratio becomes

$$\frac{\phi}{\psi} \sim 1 - i \frac{\omega_{\text{lin}} - \omega_*}{\alpha} = 1 + i \frac{\omega_{\text{lin}} k^2}{\alpha},$$

where ω_{lin} is the linear frequency $\omega_{\text{lin}} = \text{Re } \omega_{1,2}$. The condition for instability, $\Gamma \sim \text{Re} \langle ik_y \phi^* \psi \rangle > 0$ imposes a necessary condition for instability on the linear frequency ω_{lin} ,

$$0 < \omega_{\text{lin}} < \omega_*,$$

for wavenumbers $k_y > 0$.

The second-order moment equation that expresses the nonlinear conservation can be constructed as

$$\frac{dE}{dt} = \Gamma - D_{\parallel} - D_{\phi} - D_{\psi}, \quad (5)$$

where

$$E = \left\langle \frac{|\psi|^2 + |\nabla \phi|^2}{2} \right\rangle, \quad \Gamma = \kappa \langle \psi v_x \rangle = \kappa \left\langle -\psi \frac{\partial \phi}{\partial y} \right\rangle,$$

$$D_{\parallel} = \langle \alpha |\phi - \psi|^2 \rangle, \quad D_{\phi} = \langle \nu |\nabla_{\perp}^2 \phi|^2 \rangle, \quad D_{\psi} = \langle \mu |\nabla \psi|^2 \rangle.$$

The dissipation takes place through the parallel collisional damping D_{\parallel} and the perpendicular damping $D_{\phi, \psi}$.

In a steady state, the fluctuation in frequency-wavenumber $\omega - \mathbf{k}$ space is extracted from

$$\{\Phi(\mathbf{k}, \omega), \Psi(\mathbf{k}, \omega)\} = \iint dx dt e^{-i(\omega t - \mathbf{k} \cdot \mathbf{x})} \{\phi(\mathbf{x}, t), \psi(\mathbf{k}, t)\}. \quad (6)$$

An energy-like equation in the $\omega - \mathbf{k}$ basis comparable to Eq. (5) can be constructed taking the Fourier transform, multiplying the conjugates and taking the real part, to obtain

$$0 = \Gamma(\omega, \mathbf{k}) - D(\omega, \mathbf{k}) + T_{\phi}(\omega, \mathbf{k}) + T_{\psi}(\omega, \mathbf{k}), \quad (7)$$

where the expressions for nonlinear density flux Γ , parallel collisional dissipation D_{\parallel} , perpendicular viscous and diffusive dissipation D_{ϕ} and D_{ψ} , the nonlinear energy contribution T_{ϕ} from vorticity and T_{ψ} from density advection are given by

$$\Gamma(\omega, \mathbf{k}) = \kappa \text{Re} \langle ik_y \Phi \Psi^* \rangle, \quad (8a)$$

$$D(\omega, \mathbf{k}) = D_{\parallel} + D_{\phi} + D_{\psi} = \langle \alpha |\Phi - \Psi|^2 \rangle + \nu k^4 |\Phi|^2 + \mu k^2 |\Psi|^2, \quad (8b)$$

$$T_{\phi}(\omega, \mathbf{k}) = \int d\mathbf{k}' d\omega' \hat{T}_{\phi}(\omega, \mathbf{k}, \omega', \mathbf{k}'), \quad (8c)$$

$$T_{\psi}(\omega, \mathbf{k}) = \int d\mathbf{k}' d\omega' \hat{T}_{\psi}(\omega, \mathbf{k}, \omega', \mathbf{k}'). \quad (8d)$$

The integrands $\hat{T}_{\phi}(\omega, \mathbf{k}, \omega', \mathbf{k}')$ and $\hat{T}_{\psi}(\omega, \mathbf{k}, \omega', \mathbf{k}')$ are given by

$$\hat{T}_{\phi}(\omega, \mathbf{k}, \omega', \mathbf{k}') = M_{\phi}(\mathbf{k}, \mathbf{k}') \Phi^*(\omega, \mathbf{k}) \Phi^*(\omega', \mathbf{k}') \Phi^*(\omega'', \mathbf{k}'') \quad (9a)$$

$$\hat{T}_{\psi}(\omega, \mathbf{k}, \omega', \mathbf{k}') = M_{\psi}(\mathbf{k}, \mathbf{k}') \Psi^*(\omega, \mathbf{k}) [\Phi^*(\omega', \mathbf{k}') \Psi^*(\omega'', \mathbf{k}'') - \Psi^*(\omega', \mathbf{k}') \Phi^*(\omega'', \mathbf{k}'')], \quad (9b)$$

where $M_{\phi} = \hat{\mathbf{z}} \cdot \mathbf{k}' \times \mathbf{k}'' (k''^2 - k^2) / 2k^2$ and $M_{\psi} = \hat{\mathbf{z}} \cdot \mathbf{k}' \times \mathbf{k}'' / 2$, and represent nonlinear energy transfer to (ω, \mathbf{k}) by the three-mode coupling among the three spectral components, (ω, \mathbf{k}) , (ω', \mathbf{k}') , and (ω'', \mathbf{k}'') that satisfy the wave resonance conditions, $\omega + \omega' + \omega'' = 0$ and $\mathbf{k} + \mathbf{k}' + \mathbf{k}'' = 0$. The frequency relation $\omega + \omega' + \omega'' = 0$ in the $\omega - \mathbf{k}$ basis has an equal footing with the wavenumber relation $\mathbf{k} + \mathbf{k}' + \mathbf{k}'' = 0$, while the wave resonance condition for nonlinear wave coupling, $\omega(\mathbf{k}) + \omega'(\mathbf{k}') + \omega''(\mathbf{k}'') = 0$ is a function of the wavenumbers $\mathbf{k}, \mathbf{k}', \mathbf{k}''$, and is only satisfied for particular wavenumber combinations. The triple product of fluctuation fields $\sim \Phi \Phi' \Phi''$ is dependent on a complex amplitude $|\Phi \Phi' \Phi''|$ and a complex phase $\arg(\Phi \Phi' \Phi'') = -\tan^{-1}(\text{Im } \phi \phi' \phi'' / \text{Re } \phi \phi' \phi'')$.

III. NUMERICAL OBSERVATIONS

The nonlinear simulations have a grid size $(N_x \times N_y) = 256 \times 256$, and a resolution of $(\Delta k_x, \Delta k_y) = (0.1, 0.1)$. The diamagnetic parameter, viscosity, and diffusivity are fixed at $\kappa = 1$, $\nu = 0.01$, and $\mu = 0.01$. The adiabatic parameter α varies between 0.01 (hydrodynamic regime, labeled HYD), 2.0 (quasi-adiabatic regime, labeled qADI), and 10.0 (adiabatic regime, labeled ADI).

In these simulations, the conservative nonlinear term is well preserved to within an error $< 10^{-6}$, and the steady states are sustained over a sufficiently long time to allow reliable frequency analysis. Time series for each \mathbf{k} are taken with the time step $\Delta t = 0.05$, and the number of time-data samples is $N = 8000$. This gives the minimum frequency $\omega_{\text{min}} = \pi/400 \sim 0.01$. Frequency spectra are obtained by taking an ensemble average over 10 to 15 time series for each \mathbf{k} . The frequency spectra are obtained for up to $k_y = 3.2$ and the analysis is presented for $k_x = 0$.

As found in previous work,^{15,17} vortex structures of flow and density form for the hydrodynamic case $\alpha = 0.01$, as shown in the top panel of Fig. 1. Wave-like structures are not easily observed in this regime since the isotropic effect of vorticity convection dominates the anisotropy of linear drift waves. The advection of density fluctuations by velocity fluctuations produces small-scale density fluctuations around

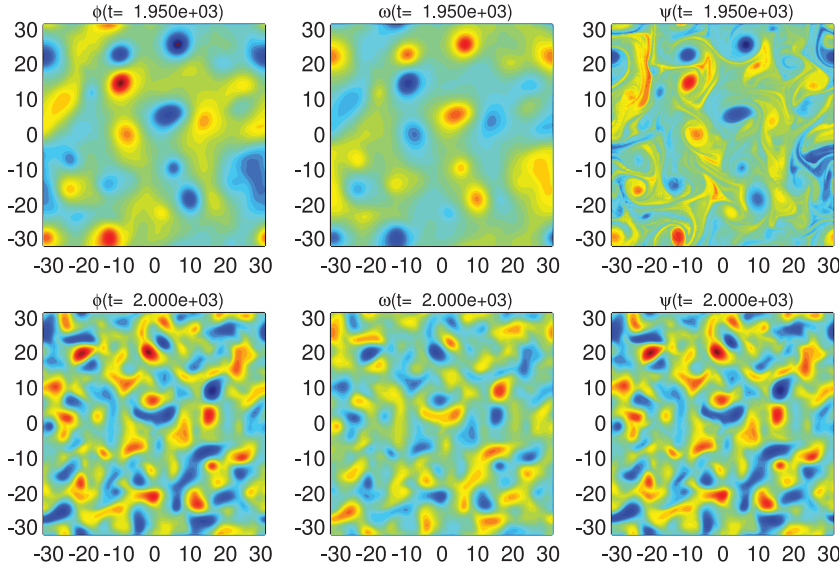


FIG. 1. The contours of electrostatic potential ϕ , vorticity ω , and density fluctuation ψ for $\alpha = 0.01$ (top) and 2.0 (bottom). The horizontal and vertical axes represent the radial and poloidal directions.

the vortex structures. This state is referred to as strong turbulence in the HW model. It is called a hydrodynamic regime because the dynamics are almost identical to hydrodynamic systems where density is advected by turbulent velocity fluctuations, as prescribed by the Navier-Stokes equation. For $\alpha = 2.0$ and above, the density fluctuations respond to the electrostatic fluctuations adiabatically, with density fluctuations following potential fluctuations according to $qE_{\parallel} - T_e \nabla_{\parallel} n_e \simeq 0$ or $\phi = \psi$. There is considerably more anisotropy for $\alpha = 2.0$ than for $\alpha = 0.01$. This state is referred to as weak turbulence in the HW model since the characteristics of linear drift waves are manifested in the cross-phases of potential and density fluctuations, and in the frequency spectrum. It is evident that the Hasegawa-Wakatani model spans weak and strong regimes of turbulence by varying only the adiabatic parameter α . In the adiabatic regime, density advection is small because $[\phi, \psi(\simeq \phi)] \approx 0$, where $[\]$ is the Poisson bracket, while in the hydrodynamic regime, the density advection may randomize the fluctuations together with vorticity advection.

The definitions of nonlinear frequency and spectral width are presented in Sec. III A and the numerical findings are shown in Secs. III B and III C.

A. A model representation of the frequency spectrum for HW turbulence

In weak turbulence theory,^{1,2,24} a correlation function of a wave takes the form

$$\langle \phi_k^*(t') \phi_k(t) \rangle = I[\omega_{\text{lin}}(\mathbf{k})] e^{-i\omega_{\text{lin}}(\mathbf{k})(t-t')}, \quad (10)$$

where $I[\omega_{\text{lin}}(\mathbf{k})]$ is the wave energy density and is proportional to the wave action of wave-kinetic theory.²⁵ In the frequency basis, the wave spectrum of Eq. (10) is

$$P(\omega) = \langle \phi_k^*(\omega) \phi_k(\omega) \rangle \propto I[\omega_{\text{lin}}(\mathbf{k})] \delta(\omega - \omega_{\text{lin}}(\mathbf{k})), \quad (11)$$

where $\delta(\omega)$ is the Kronecker delta function: $\delta(\omega) = 1$ for $\omega = 0$, otherwise $\delta(\omega) = 0$. A wave feature, $\omega = \omega_{\text{lin}}(\mathbf{k})$, is assumed. With a finite auto-correlation time $\tau_{\text{ac}} = \Delta\tilde{\omega}_k^{-1}$, the spectrum can be extended to the Lorentzian form

$$P_k^{\text{wt}}(\omega) = \langle |\phi_k(\omega)|^2 \rangle \propto \frac{\Delta\tilde{\omega}_k}{(\omega - \omega_{\text{lin}}(\mathbf{k}))^2 + \Delta\tilde{\omega}_k^2}, \quad (12)$$

where $\Delta\tilde{\omega}_k$ can be approximately taken as $\sim O(\gamma_{\ell})$ at the energetically dominant wavenumber \mathbf{k} , and γ_{ℓ} is the linear growth rate. At this wavenumber, the energy balance in a steady state requires that fluctuation energy driven by the instability be balanced by nonlinear energy damping. In the case that this nonlinear damping takes the form of spectral broadening (i.e., the resonance broadening of the wave-particle interaction^{26,27}), $\Delta\tilde{\omega}_k \sim \gamma_{\ell}$ is reasonable. This spectral form produces the auto-correlation function

$$\langle \phi_k^*(t') \phi_k(t) \rangle \propto e^{-i\omega_{\text{lin}}(\mathbf{k})(t-t') - \Delta\tilde{\omega}_k |t-t'|}.$$

Equation (12) can be generalized by replacing the linear frequency $\omega_{\text{lin}}(\mathbf{k})$ with a nonlinear frequency $\tilde{\omega}_k$, so that

$$P_k(\omega) \propto \frac{1}{\pi} \frac{\Delta\tilde{\omega}_k}{(\omega - \tilde{\omega}_k)^2 + \Delta\tilde{\omega}_k^2}. \quad (13)$$

Nonlinear frequencies $\tilde{\omega}$ are, in principal, the eigenfrequencies of a given nonlinear system and can arise out of a non-negligible nonlinear contribution from large wave amplitudes^{28,29} or out of the interaction of three waves with non-zero growth rates.¹²

In strong turbulence where the spectrum is broad, a wave feature $\omega \sim \omega_{\text{lin}}$ would not be observed due to the short auto-correlation time $\omega_{\text{lin}}(\mathbf{k}) \ll \Delta\omega_k$. The fluctuations qualitatively become quasi-random arising from nonlinear interaction,

$$P_k^{\text{st}}(\omega) \propto \frac{1}{\pi} \frac{\Delta\tilde{\omega}_k}{\omega^2 + \Delta\tilde{\omega}_k^2}.$$

For simplicity, the subscript \mathbf{k} will be dropped for the nonlinear frequency $\tilde{\omega}$ and spectral width $\Delta\tilde{\omega}$ for the rest of this paper. The Lorentzian spectral form is used only to provide a fit from which the spectral width can be extracted. Otherwise, the Lorentzian is not assumed.

A frequency spectrum

$$P_s(\omega; f_k) = \langle |f_k(\omega)|^2 \rangle, \tag{14}$$

is obtained from simulations, where $f_k(\omega)$ is the Fourier transform of $f_k(t) = [\phi_k(t), \psi_k(t)]$ and $\langle \dots \rangle$ represents the ensemble average. Assuming the Lorentzian frequency spectrum Eq. (13), a nonlinear frequency $\tilde{\omega}$ and a spectral width $\Delta\tilde{\omega}$ are estimated as

$$\tilde{\omega} = \frac{\int P_s(\omega)\omega d\omega}{\int P_s(\omega)d\omega} \quad \text{and} \quad \Delta\tilde{\omega} = \frac{\Delta\tilde{\omega}_L + \Delta\tilde{\omega}_R}{2},$$

where the left and right half-widths $\Delta\tilde{\omega}_{L,R}$ satisfy

$$\int_{\tilde{\omega}-\Delta\tilde{\omega}_L}^{\tilde{\omega}} P_s(\omega; f_k) d\omega = \int_{\tilde{\omega}}^{\tilde{\omega}+\Delta\tilde{\omega}_R} P_s(\omega) d\omega = \frac{1}{4} \int_{-\infty}^{\infty} P_s(\omega; f_k) d\omega,$$

consistent with a Lorentzian half-width. The left half-width $\Delta\tilde{\omega}_L$ and the right half-width $\Delta\tilde{\omega}_R$ differ by

$$\left| \frac{\Delta\tilde{\omega}_L - \Delta\tilde{\omega}_R}{\Delta\tilde{\omega}_L} \right| \leq 10\%.$$

Alternatively, the standard deviation of P_s could be taken as a measure of the spectral width. However, the frequency spectra of simulations are not Gaussian at the tail and the standard deviation tends to overestimate the width. While the Lorentzian nonlinear frequency and nonlinear spectral width are used to characterize the spectrum, the measured spectra can be more complicated than a Lorentzian, as shown in Fig. 2.

B. Nonlinear frequency and spectral width

In the hydrodynamic regime $\alpha = 0.01$, the frequency spectra are peaked around zero ($\tilde{\omega} \simeq 0$) and quite broad ($\Delta\tilde{\omega} \gg \tilde{\omega}$), as shown in Fig. 2(c). These frequency spectra are observed at most wavenumbers, except for the wavenumbers $k_y < 0.3$ where growth rates are maximum. In the most

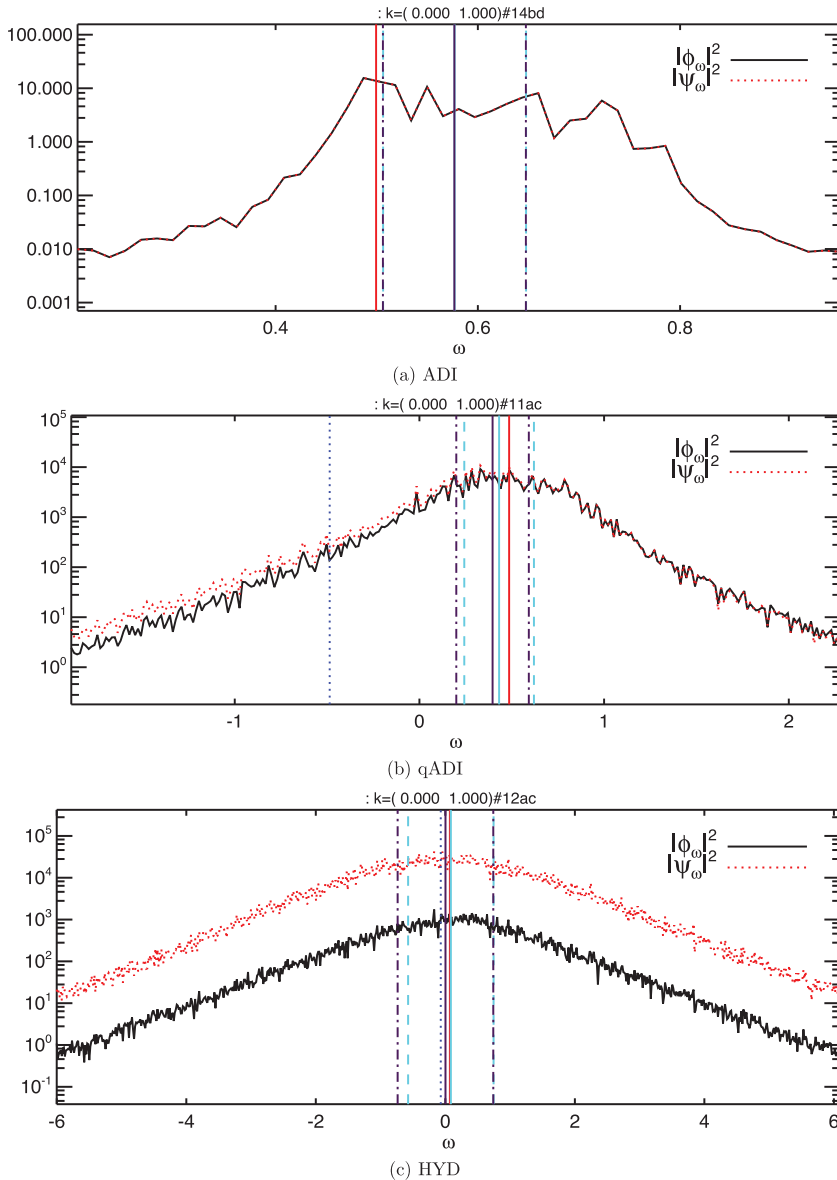


FIG. 2. Frequency spectra for $k = (0.0, 1.5)$ for (a) ADI, (b) qADI, and (c) HYD. Red (solid) and blue (dotted) vertical lines represent the linear frequencies for $\gamma > 0$ and $\gamma < 0$. Vertical cyan and magenta solid lines represent $\tilde{\omega}(\phi, \psi)$ and the spectral widths are denoted by cyan (dashed) for potential ϕ and magenta (dashed-dotted) density ψ .

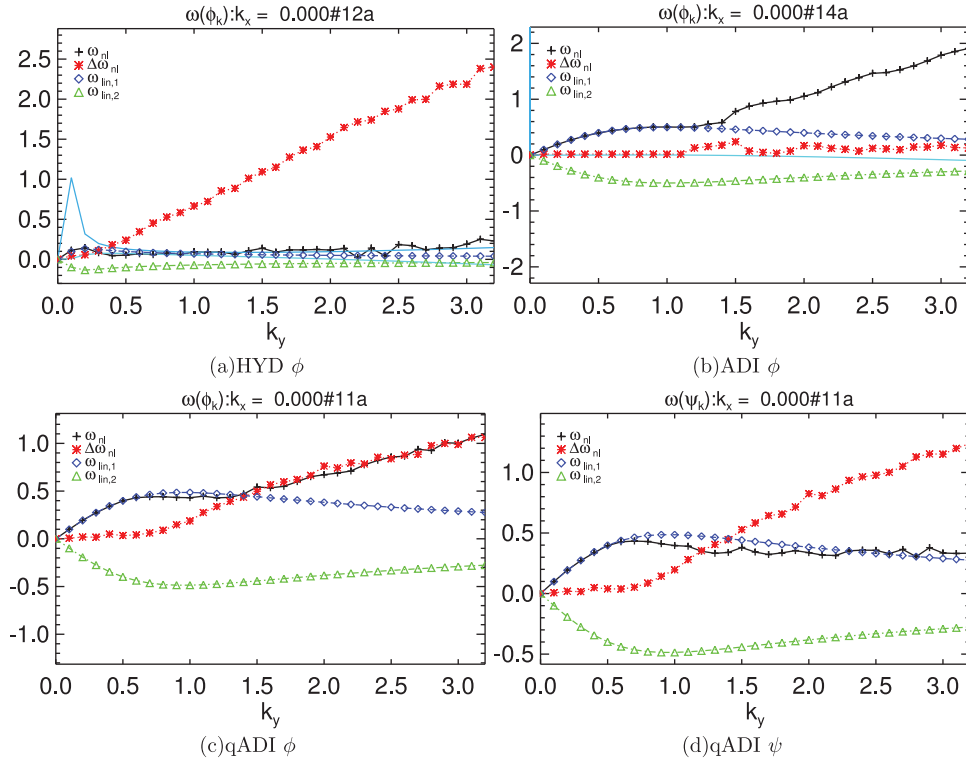


FIG. 3. Nonlinear frequency $\tilde{\omega}$ (black, +), nonlinear spectral width $\Delta\tilde{\omega}$ (red, *), linear frequency of $\omega_{lin,1}$ (blue, \diamond) and $\omega_{\ell,2}$ (green, \triangle) are plotted with the wavenumbers k_y and $k_x = 0$ for (a) potential ϕ of HYD, (b) potential ψ of ADI, (c) potential ϕ , and (d) density ψ of qADI.

unstable wavenumbers, $k_y \sim 0.2$, the nonlinear frequencies $\tilde{\omega}$ align with the linear frequencies of the unstable mode $\tilde{\omega} \sim \omega_{lin,1}$, and the spectrum is relatively narrow $\Delta\tilde{\omega} \lesssim \tilde{\omega}$, as shown in Fig. 3(a). At larger wavenumbers, the nonlinear frequencies remain finite with a value on the order of linear time scales ω_{lin} and γ_ℓ , and smaller than the spectral width $\Delta\tilde{\omega}$. The latter increases linearly with poloidal wavenumber k_y .

In the adiabatic regime of Fig. 3(b), for low k_y , the nonlinear frequencies follow the linear frequencies of the unstable mode $\tilde{\omega} \simeq \omega_{lin,1}$, as in the hydrodynamic regime. They differ only in that the wavenumber range of $\tilde{\omega} \simeq \omega_{lin,1}$ is broader since the most unstable wavenumber is $k_y \simeq 1.0$. However, the spectra at large k_y are much narrower, with $\Delta\tilde{\omega} \ll \tilde{\omega}$. This is opposite to the behavior in the hydrodynamic regime, where $\tilde{\omega} \gg \Delta\tilde{\omega}$. The nonlinear frequencies also increase linearly in wavenumber k_y , i.e., $\tilde{\omega} \propto k_y$.

While the frequency spectra of potential and density fluctuations in the hydrodynamic and adiabatic regimes are very similar, the frequency spectra of potential and density fluctuations show a different trend in the intermediate regime, $\alpha = 2.0$, as shown in Figs. 3(c) and 3(d). The nonlinear frequencies follow the linear frequencies for low and energetically dominant wavenumbers as in all the other regimes. The nonlinear frequencies of the potential fluctuations increase in k_y like the adiabatic regime, with the nonlinear broadening $\tilde{\omega} \sim \Delta\tilde{\omega}$. However, the nonlinear frequencies of the density fluctuations remain relatively flat, as in the hydrodynamic regime at the wavenumber $k_y \gtrsim 1.0$.

Summarizing these results, two clear tendencies in frequency behaviors are observed from the α scan. First, the frequency broadening and the nonlinear frequency can arise

due to the nonlinear effects, alone or together. The former is significant in the hydrodynamic regime and the latter is important in the adiabatic regime. The frequency broadening and the nonlinear frequency increase linearly in k_y . Second, for the intermediate α regime, the potential and density fluctuations differ in the nonlinear frequencies. The nonlinear frequencies for potential fluctuations tend to increase more steeply, and are larger, than those of density fluctuations. This is encapsulated in Fig. 4. As k_y increases, the nonlinear interaction appears as a nonlinear frequency shift and/or frequency broadening, depending on the nature of turbulence, weak or strong.

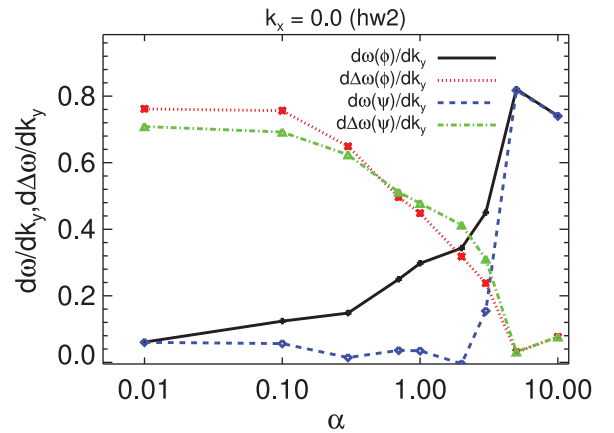


FIG. 4. The rates of change of the nonlinear frequency $d\tilde{\omega}/dk_y$ and the spectral width $d\Delta\tilde{\omega}/dk_y$ with respect to the wavenumber k_y are shown for potential and density fluctuations. Each point represent $d\omega(\phi)/dk_y$ (black, solid), $d\Delta\omega(\phi)/dk_y$ (red, dotted), $d\omega(\psi)/dk_y$ (blue, dashed), and $d\tilde{\omega}(\phi)/dk_y$ (red, dotted-dashed).

C. Cross-phase $\tilde{\theta}_{\phi\psi^*}$

The cross-phase between potential and density fluctuations is a key measure that determines particle transport given fluctuation amplitudes. The cross-phase generally shifts from the linear cross-phase set by the unstable linear eigenmode, in weakly interacting turbulence, to something that is almost random in strong turbulence. Figure 5 shows how the cross-phases change in k_y as the adiabatic parameter changes. The cross-phase of the linear modes on the unstable branch is positive. A positive cross-phase produces outward particle fluxes, even in the nonlinear case. Negative cross-phases like those of linearly stable modes produce inward particle fluxes. Quasilinear estimates of particle and thermal fluxes use the cross phase of linearly unstable modes in the range where linear instability is dominant.

The cross-phases in the nonlinear state are close to the linear cross-phases for low k_y in both the adiabatic and hydrodynamic regimes. In the hydrodynamic regime shown in Fig. 5(a), the cross-phases for low k_y match the phases of the linearly unstable modes. For larger wavenumbers, they remain approximately zero with no apparent relation to any linear cross phases, as expected. This represents a situation where the phases of density and potential fluctuations are uncorrelated and random. As α increases, the shifts of the cross-phases from linear to nonlinear values are finite, and have certain phase correlations. It should be noted that the wavenumber k_y where the cross-phases become shifted from linear values is close to the wavenumber where the nonlinear frequency $\tilde{\omega}$ becomes distinct from the linear wave frequencies. This can be clearly seen at $k_y \sim 1.2$ in Figs. 3(c) and 5(c). It is observed that the cross-phases shift negatively from the linear cross-phases at the wavenumbers where the nonlinear frequencies shift positively from linear frequencies. The frequency shift $\delta\tilde{\omega} = \tilde{\omega} - \omega_{\text{lin},\perp}$ appears definitely correlated with the cross phase $\Delta\tilde{\theta}_{\phi\psi^*} = \tilde{\theta}_{\phi\psi^*} - \theta_{\phi\psi^*,\ell,1}$.

In addition, the correlation between cross-phases and frequencies is observed in the frequency spectrum of each wavenumber. The positive shift in frequency and the negative shift in cross-phase, reflected in the relation

$$\delta\tilde{\omega}\Delta\tilde{\theta}_{\phi\psi^*} < 0, \quad (15)$$

are also observed for the individual wavenumber spectra as shown in Figs. 6(a) and 6(b). Consistent with Fig. 5(a), the cross-phase for each frequency spectrum in the hydrodynamic regime shows random phases so that the cross-phases are close to zero. This is shown in Figs. 6(c) and 6(d).

IV. FREQUENCY SPECTRUM ANALYSIS

A. Nonlinear frequency

To explain how the nonlinear frequency shift arises, the nonlinear energy contributions to the wavenumber $\mathbf{k} = (0.0, 1.0)$ by vorticity advection N_ϕ in the adiabatic regime are shown in Fig. 7. We focus on vorticity advection because density advection N_ψ is much weaker due to the adiabatic response of electron density fluctuations to the electrostatic potential fluctuation $\psi \sim \phi$. With one nonlinearity dominant the nonlinear interaction is more transparent relative to the quasi-adiabatic or hydrodynamic regimes. Figures 7(a) and 7(b) show the contribution of vorticity advection \hat{T}_ϕ in terms of

$$\hat{T}_i(k'_x, k'_y; \mathbf{k}) = \int \hat{T}_i(\omega, \mathbf{k}, \omega', \mathbf{k}') d\omega d\omega' \quad (16a)$$

$$\hat{T}_i(\omega, k'_y; \mathbf{k}) = \int \hat{T}_i(\omega, \mathbf{k}, \omega', \mathbf{k}') d\omega' dk'_x, \quad (16b)$$

where here $i = \phi$, but the same definitions apply to density advection with $i = \psi$. Positive $\hat{T}_i(\omega, \mathbf{k}, \omega', \mathbf{k}')$ represents nonlinear energy transfer from the electrostatic potential and density

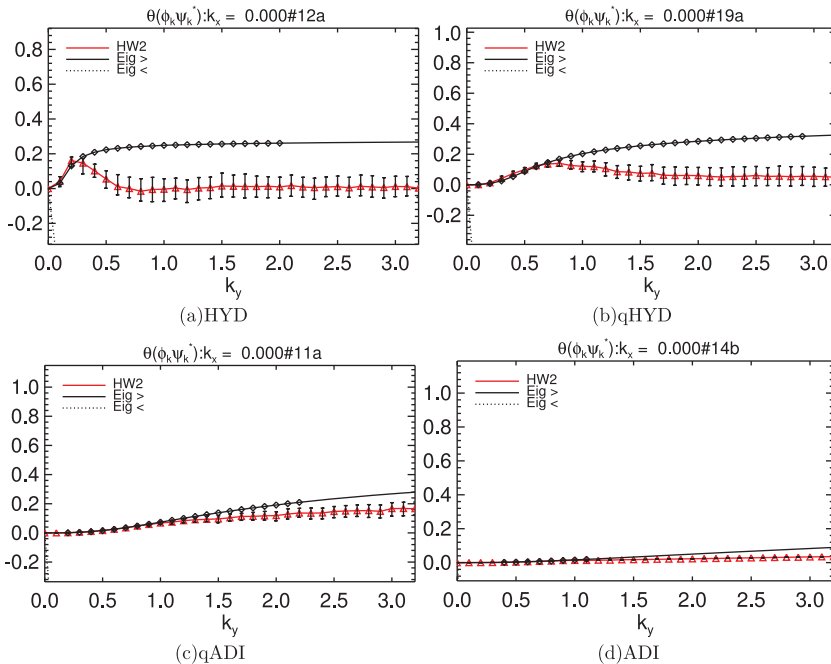


FIG. 5. Cross-phase $\langle \tilde{\theta}_{\phi\psi^*}(k_y; \alpha) \rangle$ in the poloidal wavenumber k_y for different α s (a) HYD, (b) qHYD ($\alpha = 0.3$), (c) qADI, and (d) ADI. Black lines represent the linear cross-phases (solid line: unstable; broken line: stable) and the red line with error bars represents the nonlinear cross phases computed from the simulations.

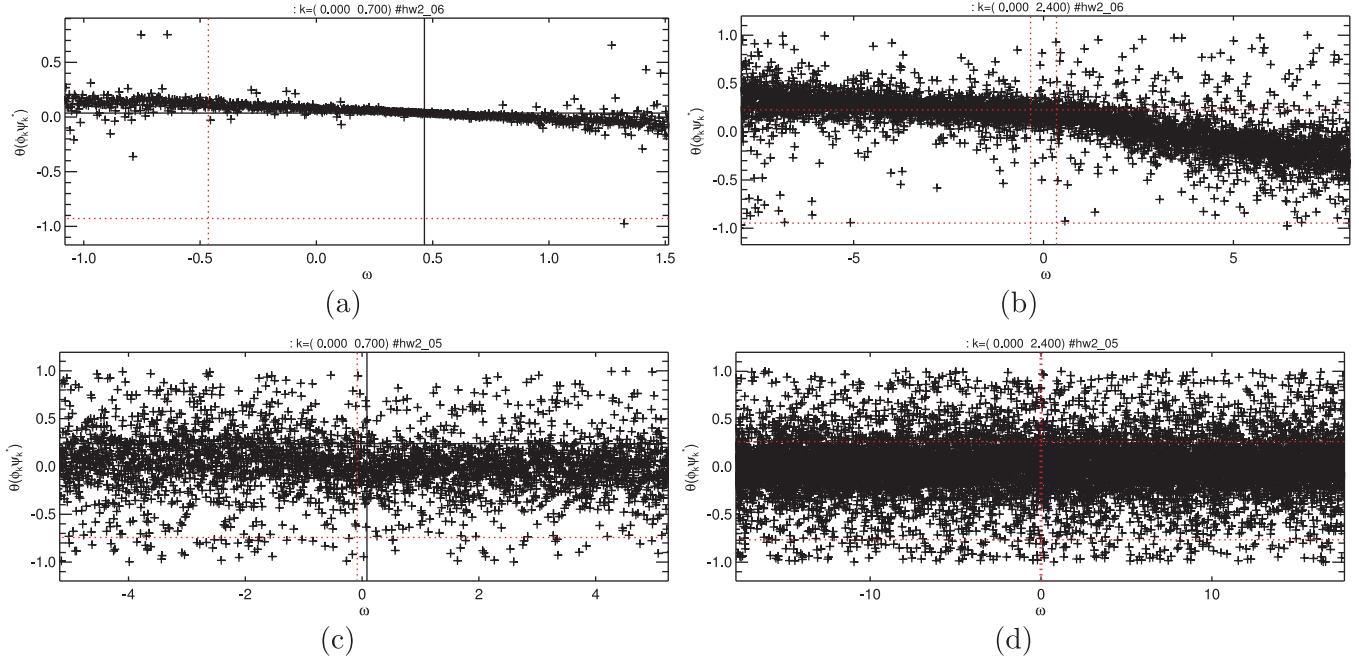


FIG. 6. Cross-phases $\tilde{\theta}_{\phi\psi}(\omega, \mathbf{k}; \alpha)$ of (a) $k_y = 0.7$; qADI (b) $k_y = 2.4$; qADI (c) $k_y = 0.7$; HYD (d) $k_y = 2.4$; HYD. The vertical lines represent linear frequencies $\omega_{\text{lin},1}$ and $\omega_{\text{lin},2}$, and the horizontal lines represent the linear cross-phases. Black (solid) and red (dotted) represent $\gamma > 0$ and $\gamma < 0$.

fluctuations at (ω', \mathbf{k}') and (ω'', \mathbf{k}'') into the i -fluctuation at (ω, \mathbf{k}) by three-wave coupling satisfying $\mathbf{k} + \mathbf{k}' + \mathbf{k}'' = 0$ and $\omega + \omega' + \omega'' = 0$. Negative $\hat{T}_i(\omega, \mathbf{k}, \omega', \mathbf{k}')$ represents nonlinear energy transfer out of the i -fluctuation at (ω, \mathbf{k}) . Figures 7(a) and 7(b) show the contours of $\hat{T}_\phi(k'_x, k'_y; \mathbf{k})$ and $\hat{T}_\phi(\omega, k'_y; \mathbf{k})$ for $\mathbf{k} = (0, 0, 1.0)$, where red indicates positive values and blue negative values. The most prominent contributions to $\mathbf{k} = (0.0, 1.0)$ from nonlinear interactions come from two triads,

- Triad I: $\mathbf{k}'_1 = (0.5, -0.7)$ and $\mathbf{k}''_1 = (-0.5, -0.3)$ and
- Triad II: $\mathbf{k}'_2 = (0.5, -0.9)$ and $\mathbf{k}''_2 = (-0.5, -0.1)$.

Except for $\mathbf{k} = (0.0, 1.0)$, the nonlinear frequencies in these two triads correspond reasonably well to the linear frequencies. The frequencies of $\hat{T}_\phi(\omega, \mathbf{k}, k'_y)$ for Triads I and II are $\omega_1 = 0.60$ and $\omega_2 = 0.48$, which are somewhat larger or similar to the linear frequency ~ 0.48 . This is because the

dispersion relation $\omega = \omega_{\text{lin},1}(\mathbf{k})$ for $k_y < 1$ has negative curvature, consistent with typical drift-wave behavior. Therefore, the frequencies of nonlinear coupling, $\omega_1 = -\omega_{\text{lin},1}(\mathbf{k}'_1) - \omega_{\text{lin},1}(\mathbf{k}''_1)$ and $\omega_2 = -\omega_{\text{lin},1}(\mathbf{k}'_2) - \omega_{\text{lin},1}(\mathbf{k}''_2)$, satisfy the approximate inequalities,

$$-\omega_{\text{lin},1}(\mathbf{k}''_2) < -\omega_{\text{lin},1}(\mathbf{k}'_1) < -\omega_{\text{lin},1}(\mathbf{k}'_1) < -\omega_{\text{lin},1}(\mathbf{k}''_2) < \omega_{\text{lin},1}(\mathbf{k}) \quad \text{and} \quad \omega_{\text{lin},1}(\mathbf{k}) < \omega_2 < \omega_1.$$

In addition, Fig. 7(b) shows that the high-frequency feature at $\omega \sim 0.6$ corresponds to energy excitation in wavevectors \mathbf{k} from the first triad while the low frequency feature at $\omega_2 \sim 0.48$ corresponds to energy loss in wavevector \mathbf{k} from the second triad. There is a feature at $\tilde{\omega} = 0.7$ representing strong excitation due to a third triad with wave vectors $\mathbf{k}'_3 = (-0.2, -0.3)$ and $\mathbf{k}''_3 = (0.2, -0.7)$. This preferential nonlinear energy transfer in the high frequency part of the

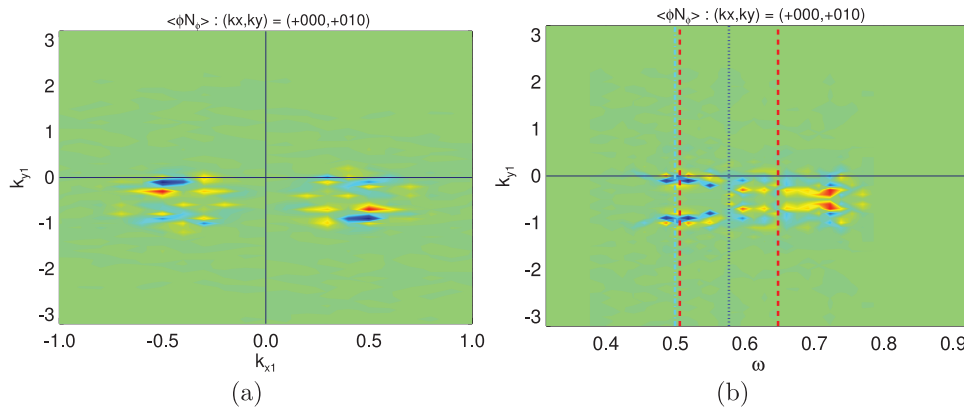


FIG. 7. The nonlinear contribution to the energy of $\mathbf{k} = (0.0, 1.0)$ in ADI by vorticity advection as functions of (a) k'_x and k'_y in $\hat{T}_\phi(\mathbf{k}, k'_x, k'_y)$ and (b) k'_y and ω in $\hat{T}_\phi(\omega, \mathbf{k}, k'_y)$. The expressions can be found in Eq. (16). The red and blue colors represent positive, $\hat{T}_\phi > 0$, and negative, $\hat{T}_\phi < 0$, energy transfer, respectively.

spectrum leads a positive nonlinear frequency shift in the potential fluctuations. Since density fluctuation is tied approximately to the potential fluctuation by strong parallel dissipation, this shift occurs in the density fluctuation. This wavenumber $\mathbf{k} = (0.0, 1.0)$ is selected because the nonlinear frequencies begin shifting from the linear frequencies at this point. At larger \mathbf{k} , more wavenumbers \mathbf{k}' are coupled to \mathbf{k} , and the features become more complex and difficult to analyze.

As α decreases, nonlinear density advection begins to make a stronger contribution to the nonlinear dynamics. In the quasi-adiabatic case, the nonlinear frequency shift is observed to be smaller in the density fluctuations than in the potential fluctuations. This smaller shift could be due to the density advection.

Figure 8 shows vorticity and density advection for the wavenumber $\mathbf{k} = (0.0, 1.5)$ in the quasi-adiabatic regime. The wavevector $\mathbf{k} = (0.0, 1.5)$ is chosen because the nonlinear frequency shift occurs in a significant way at $k_y > 1.3$. For the potential fluctuation, Figs. 8(a) and 8(b), the nonlinear transfer by vorticity advection prefers the high frequency channel as in the adiabatic case, while many more wavenumbers and frequencies are involved in the nonlinear coupling. The high frequency modes between $0.5 < \omega < 1.0$ are observed to be excited by smaller wavenumbers $|\mathbf{k}'|, |\mathbf{k}''| < |\mathbf{k}|$ (red part in Fig. 8(a)).

An increasing effect of density advection is evident in Figs. 8(c) and 8(d). While the wavenumbers contributing to

the advection in Fig. 8(c) are in a similar wavenumber range to that of Fig. 8(a), the frequency range associated with the dominant nonlinear transfer is different. The nonlinear excitation favors the low frequency region as shown in Fig. 8(d). This energy transfer produces the density fluctuation with smaller frequency shifts. In particular, the positive energy transfer to low frequencies is due to coupling with lower wavenumbers, $|\mathbf{k}| > |\mathbf{k}'|, |\mathbf{k}''|$.

The observations just presented can be compared to the inverse cascade associated with vorticity advection and the forward cascade associated with density advection. The positive energy transfer by smaller wavenumbers \mathbf{k}' to a larger wavenumber \mathbf{k} in the potential fluctuations appears to be at odds with the “inverse cascade” that statistically describes the direction of nonlinear transfer by vorticity advection in two-dimensional fluid systems.³⁰ However, the total energy transfer $\int d\omega \hat{T}_\phi(\omega, k'_y) < 0$ is actually in the direction of an inverse cascade from the negative energy transfer of triads with either $|\mathbf{k}'| < |\mathbf{k}| < |\mathbf{k}''|$ or $|\mathbf{k}''| < |\mathbf{k}| < |\mathbf{k}'|$ (blue in Fig. 8(b)). Also, the positive energy transfer due to coupling with lower wavenumbers in the density fluctuations coincides with the role of density advection, which produces a forward cascade in wavenumber space. This forward cascade occurs via the lower frequency region of the frequency spectrum.

Here, the nonlinear energy transfer to only two wavenumbers has been presented as standard cases. As density

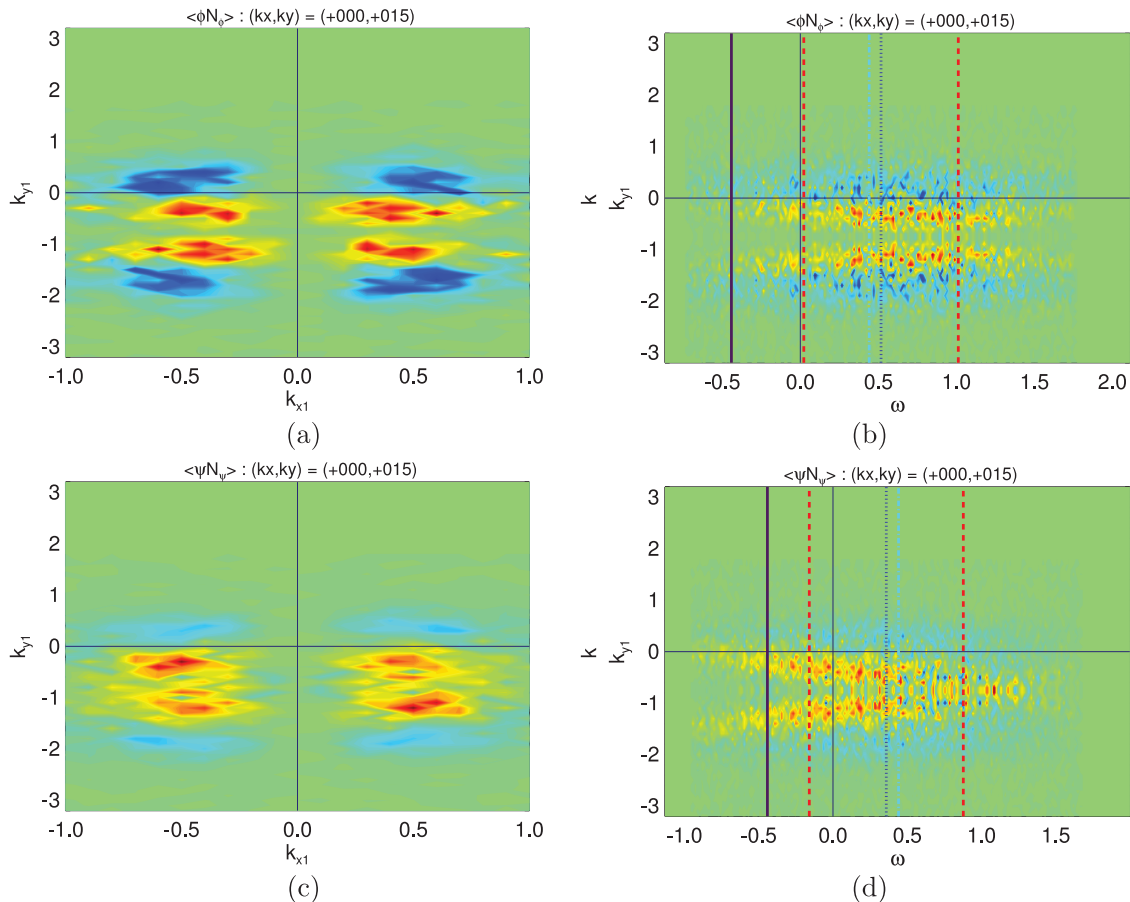


FIG. 8. The nonlinear contribution to the energy of $\mathbf{k} = (0.0, 1.5)$ in qADI by vorticity advection (a) $\hat{T}_\phi(k'_x, k'_y)$ and (b) $\hat{T}_\phi(\omega, k'_y)$, and density advection (c) $\hat{T}_\psi(k'_x, k'_y)$ and (d) $\hat{T}_\psi(\omega, k'_y)$. The expressions can be found in Eq. (16). The color schemes are the same as in Fig. 7.

advection becomes stronger and wavenumbers larger, the relation between the nonlinear transfer and nonlinear frequencies becomes less clear than these standard cases. Nevertheless, the trends described in the standard cases are observed qualitatively for wavenumbers where a nonlinear frequency shift is observed. The energy transfer to larger wavenumbers by vorticity advection prefers the high-frequency channel to the low-frequency channel in energy transfer to larger wavenumbers. This results in a nonlinear frequency shift to higher frequency. And the density advection cascades energy in the forward direction through low frequency space, and that energy transfer correlates with low nonlinear frequency as k_y increases. Therefore, as α decreases, density advection becomes the dominant nonlinear process, which leads to frequency that is approximately zero at large k .

B. Cross-phase $\tilde{\theta}_{\phi\psi^*}$

To investigate the cross-phase observations described in Sec. III C, a different approach is taken from the energetics analysis given above. Consider for the moment a one-field equation, which generally can be written in the form

$$\frac{\partial \phi}{\partial t} = L\phi + M\phi\phi. \quad (17)$$

Taking the Fourier series and using Φ to designate the Fourier expansion of ϕ , Φ can be expressed in terms of a linear response R and source functions N

$$\Phi(\omega, \mathbf{k}) = R(\omega, \mathbf{k})N(\omega, \mathbf{k}), \quad (18)$$

where

$$R(\omega, \mathbf{k}) = -\frac{1}{i\omega + L_{\mathbf{k}}}$$

$$N(\omega, \mathbf{k}) = \int M(\mathbf{k}, \mathbf{k}')\Phi^*(\omega', \mathbf{k}')\Phi^*(\omega'', \mathbf{k}'')d\mathbf{k}'d\omega'.$$

We write the two-field HW equations in a similar form, but use the linear eigen-frequencies ω_i and eigenvectors β_i to express the linear terms. The HW equations in $\omega - \mathbf{k}$ space assume the following form (see the Appendix for details):

$$\begin{aligned} \Phi &= \frac{i}{\beta_2 - \beta_1} \left[\left(\frac{\beta_2}{\omega - \omega_1} + \frac{-\beta_1}{\omega - \omega_2} \right) N_\phi \right. \\ &\quad \left. + \left(\frac{-1}{\omega - \omega_1} + \frac{1}{\omega - \omega_2} \right) N_\psi \right] \\ \Psi &= \frac{i}{\beta_2 - \beta_1} \left[\left(\frac{\beta_1\beta_2}{\omega - \omega_1} + \frac{-\beta_1\beta_2}{\omega - \omega_2} \right) N_\phi \right. \\ &\quad \left. + \left(\frac{-\beta_1}{\omega - \omega_1} + \frac{+\beta_2}{\omega - \omega_2} \right) N_\psi \right], \end{aligned} \quad (19)$$

where Φ and Ψ are the Fourier transforms of ϕ and ψ defined in Eq. (6), and β_i represents the density component of the i th eigenmode, normalized by the electrostatic potential part of the eigenmode, as shown in Eq. (A6). The nonlinear terms (N_ϕ, N_ψ) are

$$\begin{aligned} N_\phi &= -\frac{1}{2} \sum' \hat{z} \cdot \mathbf{k}' \times \mathbf{k}'' \frac{(k'^2 - k''^2)}{k^2} \Phi'^* \Phi''^* \quad \text{and} \\ N_\psi &= \frac{1}{2} \sum' \hat{z} \cdot \mathbf{k}' \times \mathbf{k}'' (\Phi' \Psi'' - \Psi' \Phi''). \end{aligned} \quad (20)$$

Solutions of the nonlinear system in $\omega - \mathbf{k}$ space do not correspond to linear modes (unstable or stable) in general. The response proportional to the pole $(\omega - \omega_i)^{-1}$ represents a stationary linear response that resonates at the frequency $\text{Re } \omega_i$ with the spectral width $\text{Im } \omega_i$, giving rise to the phase $\arg \beta_i$ in relation to an arbitrary source. Although this formulation is formally exact, its interpretation as a response function is worth further investigation using a proper complex analysis. While an appropriate response function satisfies a causality relation,³¹ the apparent presence in the denominator of both positive and negative growth rates $\text{Im } \omega_i$ for the steady state requires further consideration.

Putting aside the nuances of complex analysis and causality, the expressions of Eq. (19) describe the cross-phase behavior and its relation to frequency in a transparent fashion. We obtain a linear relation between the density and potential fluctuations for the limit in which vorticity advection dominates, $|N_\phi| \gg |N_\psi|$, which corresponds to the adiabatic case. Consider for the moment a response restricted to the unstable root $(\omega - \omega_1)^{-1}$, which produces the cross phase β_1 of Eq. (4). This cross-phase belongs to the linearly unstable mode for each \mathbf{k} regardless of frequency. A variation of the cross-phase in frequency space would not be expected. However, inclusion of the stable root leads to the complex ratio Φ/Ψ ,

$$\frac{\Phi}{\Psi} = \beta_1 \left(1 - \frac{\omega - \omega_1}{\omega - \omega_2} \right) / \left(1 - \frac{\beta_1 \omega - \omega_1}{\beta_2 \omega - \omega_2} \right), \quad (21)$$

and associated cross-phase $\theta_{\phi\psi^*}$,

$$\begin{aligned} \theta_{\phi\psi^*}(\omega, \mathbf{k}) &= -\arg(\beta_1) - \arg \left(1 - \frac{\omega - \omega_1}{\omega - \omega_2} \right) \\ &\quad + \arg \left(1 - \frac{\beta_1 \omega - \omega_1}{\beta_2 \omega - \omega_2} \right), \end{aligned} \quad (22)$$

where for each \mathbf{k} , the cross-phase between the density and potential fluctuations varies with frequency ω . Moreover, Eqs. (21) and (22) can be further approximated in the adiabatic regime by assuming $|\beta_2| \gg |\beta_1|$, $|\gamma_2| \gg |\gamma_1|$ in order to bring out more clearly the effect of the linearly stable response. Near the frequency of the linearly unstable branch $\Re \omega_1$ where $\delta\omega = \omega - \Re \omega_1(\mathbf{k})$, Eqs. (21) and (22) become

$$\frac{\Psi}{\Phi} \simeq \beta_1 \left(1 - \frac{\delta\omega - i\gamma_1}{(\Re \omega_1 - \Re \omega_2) - i\gamma_2} \right) \simeq \beta_1 e^{-\frac{\delta\omega - i\gamma_1}{(\Re \omega_1 - \Re \omega_2) - i\gamma_2}} \quad \text{and} \quad (23)$$

$$\theta_{\phi\psi^*}(\omega, \mathbf{k}) \simeq -\arg(\beta_1) + \frac{\gamma_2 \delta\omega}{(\Re \omega_1 - \Re \omega_2)^2 + \gamma_2^2}. \quad (24)$$

Since $\gamma_2 < 0$, the cross-phase estimate qualitatively provides the means for understanding the empirical behavior

summarized in Eq. (15), which indicates that the cross-phase shifts negatively as frequency increases.

In Figs. 9 and 10, the cross-phase described by Eq. (22) (not the approximated version of Eq. (24)) is compared with the cross-phases calculated from the simulations. Figure 9 shows the comparison for wavenumbers between $k_y = 0.5$ and 3.0 in the adiabatic regime. Except for $k_y = 0.5$, the cross-phases derived from the linear calculation fit extremely well with the cross-phases from the simulation, especially within the spectral widths, denoted by the vertical dotted lines in Fig. 9, where the fluctuation amplitudes are significant. At $\omega = \omega_{lin,1}$, denoted by the vertical red (solid) lines in Figs. 9(a) and 9(b) and blue (dotted) line in Fig. 9(c), the cross-phases match well those of the linearly unstable modes. The linear frequencies $\omega_{lin,1}$ in Figs. 9(d)–9(f) are far smaller than the nonlinear frequencies and are not shown in the figures.

Figure 10 shows the comparison in the quasi-adiabatic regime. The estimate given by Eq. (22) approximately follows the cross-phase above the nonlinear frequency, $\omega > \tilde{\omega}(\phi)$.

For $k_y = 0.5$ and 1.0, the cross-phase deviates from the linear estimates. A possible cause is nonlinear density advection N_ψ , which is not included in the estimates. The nonlinear density advection N_ψ absent in Eq. (22) is no longer weak and negligible in this regime. Density advection is more critical in the frequency range $\omega < \tilde{\omega}(\phi)$ because it favors the low-frequency part of the spectrum in its energy transfer, as discussed in Sec. IV A.

C. Discussion

The correlation of the nonlinear frequency shift with the cross-phase shift in the saturated state of the adiabatic regime can be appreciated from the energy equation, Eq. (5). Negative cross-phases correlated with positive nonlinear frequency produce a smaller density flux Γ in the frequency range where the amplitudes $\Phi(\omega, \mathbf{k})$ do not vary significantly. Since the density flux is the only injection term in the turbulent energy equation, the flux injects less energy into the fluctuations than in the purely unstable linear state. In the

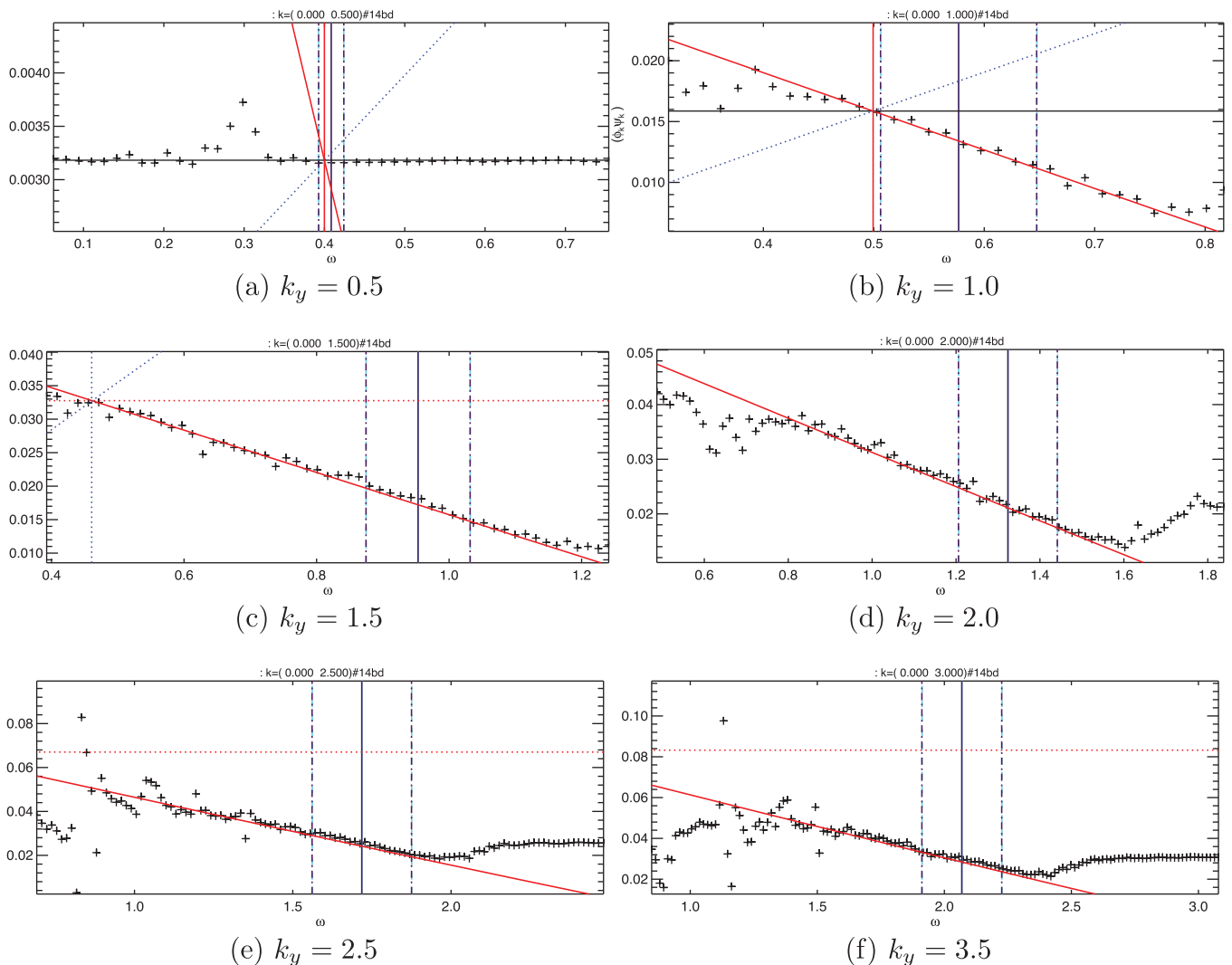


FIG. 9. Cross-phases $\theta_{\phi\psi^*}$ (black,+) in ADI are compared to the estimates by Eq. (22) (red, solid). From the top left to bottom right, the figures are shown for $k_y = 0.5, 1.0, 1.5, 2.0, 2.5, 3.0$. Black (solid) and red (dotted) horizontal lines represent the linear cross-phases for $\gamma > 0$ and $\gamma < 0$. Vertical lines are the same as in Fig. 2. In the adiabatic regime, the nonlinear frequency and the spectral widths for potential and density fluctuations are the same.

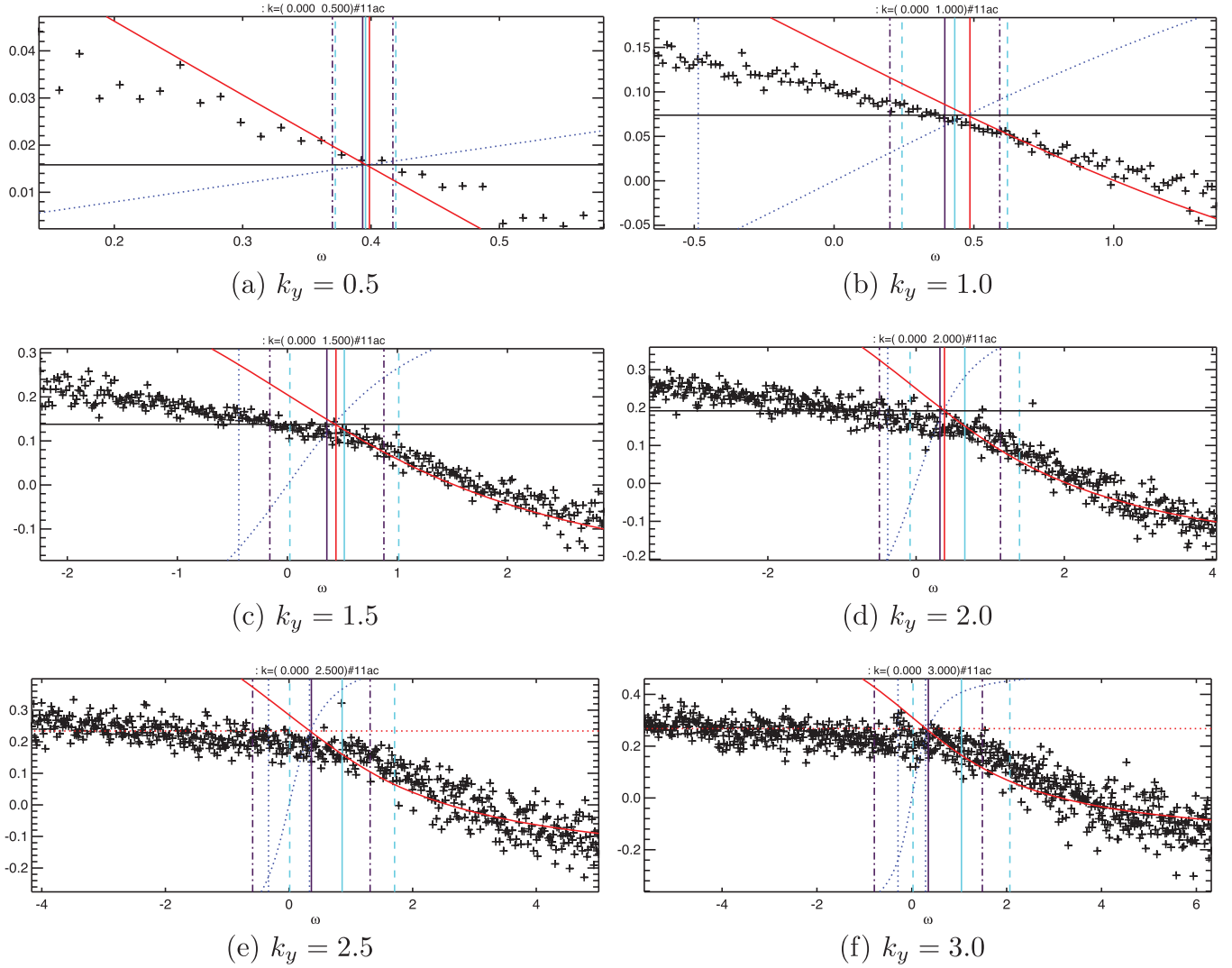


FIG. 10. The same plots are shown for qADI.

adiabatic case, it is observed that the energy is damped at the larger frequencies $\omega > \bar{\omega}(\mathbf{k})$ for unstable wavenumbers, and stronger damping is numerically observed at still larger wavenumbers where no linearly unstable modes exist. This implies that the nonlinear frequency shift can provide a way to saturate the nonlinear state created by density-driven turbulence without large frequency broadening.

Also, this correlation suggests that the relationship between the HM^{23,32} and the Hasegawa-Wakatani models is worth reassessing. While the Hasegawa-Wakatani model in the adiabatic limit can be asymptotically reduced to the Hasegawa-Mima model, the Hasegawa-Mima model shows strong turbulence³³ while the Hasegawa-Wakatani model shows weak turbulence in the same limit. This apparent contradiction can be attributed to the role of the cross-phase between the density and potential fluctuations. Even though the density fluctuation is slaved to the potential fluctuation, the absence of an independent density fluctuation in the HM model misses key dynamics of the cross-phase, which maintains density and potential fluctuations in this extended linear phase. The absence of the cross-phase in the dynamics may cause the nonlinear interaction to appear only as nonlinear diffusion, not as a nonlinear frequency shift.

As shown in Sec. IV B, the response of the stable root in the Hasegawa-Wakatani model gives rise to the dependence of cross-phases on frequency in the adiabatic and quasi-adiabatic regimes. In these regimes, the energy analysis based on unstable and stable linear modes^{6,9,10} has shown that the linearly stable modes play an insignificant role in the nonlinear density fluxes and saturation in the adiabatic regime.¹⁰ While our finding emphasizes a linearly stable response, its effect on the total density flux in the adiabatic regime is negligible because linearly stable responses gives a small change in the cross-phase at low wavenumbers $k_y \lesssim 1.0$. However, the nature of quasilinear estimates, or the role of energetically dominant modes in the nonlinear balance, may need rethinking; this frequency shift and the linear cross-phase derived in Eq. (22) may need to be taken into account in simple transport modeling or any subgrid modeling, because the level of transport and the amplitudes are determined through the energy balance, including at large wavenumbers.

There is distinct asymmetry in the frequency spectrum of each \mathbf{k} and the linear and nonlinear interactions in the adiabatic regime. Since the cross-phase decreases with frequency in the adiabatic and quasi-adiabatic regimes, the

density flux Γ , which is proportional to the cross-phase, decreases too. Moreover, the observed ratio of amplitudes Φ/Ψ is close to the adiabatic response (or the amplitudes of the linearly unstable branch) at positive $\delta\omega$, and tends to be small at the negative $\delta\omega$. Therefore, $\Gamma \sim \sin\tilde{\theta}_{\phi\psi^*}$, and the parallel dissipation $D_{\parallel} \sim |\phi - \psi|$ is smaller at positive $\delta\omega$ than at negative $\delta\omega$.

V. CONCLUSIONS

The frequency spectra at each wavenumber in the HW model are investigated in terms of a nonlinear frequency, a spectral width, and a cross-phase. In the hydrodynamic regime, a simple broadening of the spectra is observed with almost zero nonlinear frequency, as expected in strong turbulence. In the adiabatic regime, a significant nonlinear frequency shift in the electron drift direction is observed and the nonlinear frequencies increase linearly with poloidal wavenumber k_y . The spectra show that the spectral width $\Delta\tilde{\omega}$ is smaller than the nonlinear frequency $\tilde{\omega}$ even at large wavenumbers where the wavenumbers interact nonlinearly. Therefore, these observations show that the nonlinear interactions can manifest themselves as a nonlinear frequency as well as spectral broadening.

Emerging nonlinear frequencies for density and potential fluctuations can be explained by three-wave nonlinear interaction with a combination of vorticity and density advection. The change of the cross-phase in frequency can be explained by the relation between frequency and phase via linear drift waves including the linearly stable response. Investigating the nonlinear energy transfer, it is found that vorticity advection is correlated with the frequency shift in the adiabatic regime, since wave coupling excites high frequencies near the end of the dominant energy range. The frequency shift is propagated through mode couplings to larger wavenumbers. In the intermediate regime, the nonlinear frequencies for density fluctuations are observed to be smaller than those of potential fluctuations. Density advection is attributed to the smaller nonlinear shift of density fluctuations because the forward cascade favors the low frequency channel. This line of reasoning describes numerical simulations showing that the nonlinear frequency becomes zero as simulations go to the hydrodynamics limit.

In the adiabatic regime, the cross-phase shift $\Delta\tilde{\theta}_{\phi\psi^*}(\omega, \mathbf{k})$ between potential and density fluctuations is anti-correlated with the nonlinear frequency shift $\delta\omega = \omega - \omega_{\text{lin}}(\mathbf{k})$, i.e., $\Delta\tilde{\theta}_{\phi\psi^*}(\omega, \mathbf{k})\delta\omega < 0$. This correlation fits well into a linear relation, not from linearly unstable modes alone, but arising from the full response of unstable and stable roots in the dispersion relation.

All the findings are likely to be inter-related with each other and self-consistently explained within a single framework. For that purpose, a nonlinear response function should be more rigorously developed with use of a two-point closure³ so that the cross-phase and the level of the amplitudes can be consistently connected along with the nonlinear terms, N_{ϕ} and N_{ψ} . Future work will give an answer to the quantitative description of the frequency shift and the linear

relation of the spectral width and the frequency shift for fixed wavenumber k_y .

ACKNOWLEDGMENTS

This work was supported by Department of Energy Grant No. DE-FG02-089ER53291. In addition, the author (J.H.K.) acknowledges the support of the World Class Institute (WCI) Program of the National Research Foundation of Korea(NRF) funded by the Ministry of Education, Science and Technology of Korea (MEST) (NRF Grant No. WCI 2009-001, Project No. N01130561), for helping him finishing this article.

APPENDIX: HW EQUATION IN $\omega - k$ SPACE

The HW equations in $\omega - k$ space can be written as

$$-i\omega\bar{\Phi} = \bar{L}\bar{\Phi} + \bar{N}. \quad (\text{A1})$$

Since \bar{L} is a non-Hermitian matrix, the orthogonality condition satisfies $\bar{U}\bar{L}\bar{V} = \bar{\lambda}$, where \bar{U} and \bar{V} are left and right eigen matrices and $\bar{\lambda}$ is the eigenvalue matrix. The linear matrix \bar{L} can be expressed using the orthogonality relation, $\bar{U}\bar{V} = \bar{I}$ as follows:

$$\bar{L} = \bar{U}^{-1}\bar{\lambda}\bar{V}^{-1} = \bar{V}\bar{\lambda}\bar{U}. \quad (\text{A2})$$

The HW equations are then written as

$$-i\tilde{\omega}\bar{\Phi} = \bar{V}\bar{\lambda}\bar{U}\bar{\Phi} + \bar{N}. \quad (\text{A3})$$

The inversion yields

$$\bar{\Phi} = \bar{V}(-i\tilde{\omega} - \bar{\lambda})^{-1}\bar{U}\bar{N}, \quad (\text{A4})$$

where

$$\tilde{\omega} = \omega\bar{I}. \quad (\text{A5})$$

Without loss of generality, we can define \bar{V} , which in turn determines \bar{U}

$$\bar{V} = \begin{pmatrix} 1 & 1 \\ \beta_1 & \beta_2 \end{pmatrix} \quad \text{and} \quad \bar{U} = \frac{1}{\beta_2 - \beta_1} \begin{pmatrix} \beta_2 & -1 \\ -\beta_1 & 1 \end{pmatrix}, \quad (\text{A6})$$

where β_i represents ψ/ϕ for an eigenvalue $\lambda_i = -i\omega_i$.

$$\begin{aligned} (-i\tilde{\omega} - \bar{\lambda})^{-1} &= \begin{pmatrix} -i(\omega - \omega_1) & 0 \\ 0 & -i(\omega - \omega_2) \end{pmatrix}^{-1} \\ &= i \begin{pmatrix} \frac{1}{\omega - \omega_1} & 0 \\ 0 & \frac{1}{\omega - \omega_2} \end{pmatrix}. \end{aligned} \quad (\text{A7})$$

Then the fluctuation fields in the wavenumber-frequency space are

$$\begin{aligned}
\bar{\Phi} &= \frac{i}{\beta_2 - \beta_1} \begin{pmatrix} 1 & 1 \\ \beta_1 & \beta_2 \end{pmatrix} \begin{pmatrix} \frac{1}{\omega - \omega_1} & 0 \\ 0 & \frac{1}{\omega - \omega_2} \end{pmatrix} \begin{pmatrix} \beta_2 & -1 \\ -\beta_1 & 1 \end{pmatrix} \bar{N} \\
&= \frac{i}{\beta_2 - \beta_1} \begin{pmatrix} \frac{1}{\omega - \omega_1} & \frac{1}{\omega - \omega_2} \\ \frac{\beta_1}{\omega - \omega_1} & \frac{\beta_2}{\omega - \omega_2} \end{pmatrix} \begin{pmatrix} \beta_2 & -1 \\ -\beta_1 & 1 \end{pmatrix} \bar{N} \\
&= \frac{i}{\beta_2 - \beta_1} \begin{pmatrix} \frac{\beta_2}{\omega - \omega_1} + \frac{-\beta_1}{\omega - \omega_2} & \frac{-1}{\omega - \omega_1} + \frac{1}{\omega - \omega_2} \\ \frac{\beta_1\beta_2}{\omega - \omega_1} + \frac{-\beta_1\beta_2}{\omega - \omega_2} & \frac{-\beta_1}{\omega - \omega_1} + \frac{+\beta_2}{\omega - \omega_2} \end{pmatrix} \bar{N}.
\end{aligned}$$

These yield the expressions

$$\begin{aligned}
\Phi &= \frac{i}{\beta_2 - \beta_1} \left[\left(\frac{\beta_2}{\omega - \omega_1} + \frac{-\beta_1}{\omega - \omega_2} \right) N_\phi \right. \\
&\quad \left. + \left(\frac{-1}{\omega - \omega_1} + \frac{1}{\omega - \omega_2} \right) N_\psi \right], \\
\Psi &= \frac{i}{\beta_2 - \beta_1} \left[\left(\frac{\beta_1\beta_2}{\omega - \omega_1} + \frac{-\beta_1\beta_2}{\omega - \omega_2} \right) N_\phi \right. \\
&\quad \left. + \left(\frac{-\beta_1}{\omega - \omega_1} + \frac{+\beta_2}{\omega - \omega_2} \right) N_\psi \right].
\end{aligned}$$

¹R. Z. Sagdeev and A. A. Galeev, *Nonlinear Plasma Theory* (Benjamin, New York, 1969).

²V. E. Zakharov, V. S. L'vov, and G. E. Falkovich, *Kolmogorov Spectral of Turbulence I—Wave Turbulence, Series in Nonlinear Dynamics* (Springer-Verlag, 1992).

³J. A. Krommes, *Phys. Rep.* **360**, 1 (2002).

⁴R. H. Kraichnan, *Phys. Fluids* **6**, 1603 (1963).

⁵N. Mattor and P. W. Terry, *Phys. Fluids B* **4**, 1126 (1992).

⁶D. R. Hatch, P. W. Terry, W. M. Nevins, and W. Dorland, *Phys. Plasmas* **16**, 022311 (2009).

⁷T. Gorler and F. Jenko, *Phys. Plasmas* **15**, 102508 (2008).

⁸P. W. Terry, D. A. Baver, and S. Gupta, *Phys. Plasmas* **13**, 022307 (2006).

⁹J.-H. Kim and P. W. Terry, *Phys. Plasmas* **17**, 112306 (2010).

¹⁰K. Makwana, P. W. Terry, J.-H. Kim, and D. R. Hatch, *Phys. Plasmas* **18**, 012302 (2011).

¹¹D. R. Hatch, P. W. Terry, F. Jenko, F. Merz, and W. M. Nevins, *Phys. Rev. Lett.* **106**, 115003 (2011).

¹²J.-H. Kim and P. W. Terry, *Phys. Plasmas* **18**, 092308 (2011).

¹³M. Xu, G. R. Tynan, P. H. Diamond, P. Manz, C. Holland, N. Fedorczak, S. C. Thakur, J. H. Yu, K. J. Zhao, and J. Q. Dong *et al.* (HL-2A Team), *Phys. Rev. Lett.* **108**, 245001 (2012).

¹⁴A. Hasegawa and M. Wakatani, *Phys. Rev. Lett.* **50**, 682 (1983).

¹⁵F. Y. Gang, P. H. Diamond, J. A. Crotinger, and A. E. Koniges, *Phys. Fluids B* **3**, 955 (1991).

¹⁶S. A. Orszag, *J. Fluid Mech.* **41**, 363 (1970).

¹⁷G. Hu, J. A. Krommes, and J. C. Bowman, *Phys. Plasmas* **4**, 2116 (1997).

¹⁸R. H. Kraichnan, *Phys. Rev.* **109**, 1407 (1958).

¹⁹R. H. Kraichnan, *Phys. Fluids* **8**, 575 (1965).

²⁰S. Futatani, W. J. T. Bos, D. del-Castillo-Negrete, K. Schneider, S. Benkadda, and M. Farge, *C. R. Phys.* **12**, 123 (2011).

²¹A. Hasegawa and M. Wakatani, *Phys. Rev. Lett.* **59**, 1581 (1987).

²²P. Terry and W. Horton, *Phys. Fluids* **25**, 491 (1982).

²³A. Hasegawa and K. Mima, *Phys. Fluids* **21**, 87 (1978).

²⁴A. Yoshizawa, S.-I. Itoh, K. Itoh, and N. Yokoi, *Plasma Phys. Controlled Fusion* **43**, R1 (2001).

²⁵P. H. Diamond, M. N. Rosenbluth, F. L. Hinton, M. Malkov, J. Fleischer, and A. Smolyakov, in 17th IAEA Fusion Energy Conference (International Atomic Energy Agency, Vienna, 1998), pp. IAEA-CN-69/TH3/1.

²⁶T. H. Dupree, *Phys. Fluids* **9**, 1773 (1966).

²⁷T. H. Dupree, *Phys. Fluids* **10**, 1049 (1967).

²⁸F. Hinton and W. Horton, *Phys. Fluids* **14**, 116 (1971).

²⁹G. J. Morales and T. M. O'Neil, *Phys. Rev. Lett.* **28**, 417 (1972).

³⁰R. H. Kraichnan and D. Montgomery, *Rep. Prog. Phys.* **43**, 547 (1980).

³¹G. B. Arfken and H. J. Weber, *Mathematical Methods for Physicists* (Academic Press, 2001).

³²A. Hasegawa and K. Mima, *Phys. Rev. Lett.* **39**, 205 (1977).

³³M. Ottaviani and J. A. Krommes, *Phys. Rev. Lett.* **69**, 2923 (1992).